On the normal modes of free vibration of inhomogeneous and anisotropic elastic objects

William M. Visscher, Albert Migliori, Thomas M. Bell, and Robert A. Reinert
Los Alamos National Laboratory, Los Alamos, New Mexico 87545

(Received 5 April 1991; accepted for publication 23 June 1991)

The Hamilton's principle approach to the calculation of vibrational modes of elastic objects with free boundaries is exploited to compute the resonance frequencies of a variety of anisotropic elastic objects, including spheres, hemispheres, spheroids, ellipsoids, cylinders, eggs, shells, bells, sandwiches, parallelepipeds, cones, pyramids, prisms, tetrahedra, octahedra, and potatoes. The paramount feature of this calculation, which distinguishes it from previous ones, is the choice of products of powers of the Cartesian coordinates as a basis for expansion of the displacement in a truncated complete set, enabling one to analytically evaluate the required matrix elements for these systems. Because these basis functions are products of powers of x, y, and z, this scheme is called the xyz algorithm. The xyz algorithm allows a general anisotropic elastic tensor with any position dependence and any shape with arbitrary density variation. A number of plots of resonance spectra of families of elastic objects are displayed as functions of relevant parameters, and, to illustrate the versatility of the method, the measured resonant frequencies of a precision machined but irregularly shaped sample of aluminum (called a potato) are compared with its computed normal modes. Applications to materials science and to seismology are mentioned.

PACS numbers: 43.20.Ks, 43.40.At

INTRODUCTION

Some years ago, it was noticed by Holland[1] and Demarest[2,3] that a very simple variational principle can be used to derive an eigenvalue equation for the normal-mode frequencies and eigenvectors for the vibrations of an elastic body with free boundaries. Subsequently Ohno[4] and others[5-8] have refined this method and its application to the resonant ultrasonic determination of elastic constants of materials, using small rectangular parallelepipedal single-crystal samples. The idea is illustrated in Fig. 1, which shows a crystal suspended between two transducers, one of which excites the sample, and the other measures its response. Others have used spheres,[9,10] again single-crystals with anisotropic elastic tensors (with orthorhombic or better symmetry). Spheres have the advantage that it becomes unnecessary (indeed, impossible) to align the faces of the sample with crystal axes. It is the purpose of the present paper to present a simple computational scheme with which the free vibrations of all the systems that have been analyzed up to now can be computed, and to give results for some new systems. We have fabricated a sample of one of these new systems, and have measured and computed its resonant frequencies.

I. THE METHOD

A. Motivation

It is reasonable to expect that, if one knew all the normal-mode frequencies of an elastic object, one could deduce all of the relevant properties of that object, including, up to a common scale factor, its elastic tensor and density (including their spacial variations), and its shape. Whether this is rigorously true, even for such a simple system as a two-dimensional elastic membrane, is still an unsolved problem in applied mathematics.[11] In practice, resonant ultrasonic methods have been developed, and are still being refined in significant ways,[12] which promise to become benchmark procedures for measuring these material properties. In order to exploit these ideas, it is necessary to develop a computational scheme to obtain the material parameters from measured frequencies. The procedures that have been proposed and implemented to do this generally involve defining a figure of merit F, such as the mean-square deviation of the measured from the computed resonant frequencies. Minimizing F always involves some kind of a search in the space of the relevant material parameters (elastic constants, density, dimensions, shape parameters), which requires repeated computations of the frequencies for different values of those parameters. Thus an essential part of a viable procedure is an accurate method to compute normal modes,

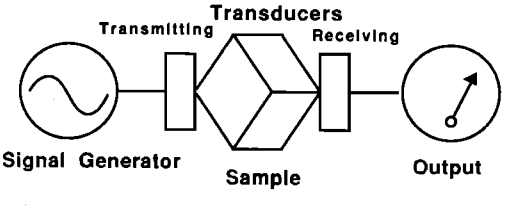

FIG. 1. Schematic resonant ultrasound setup. The sample, a rectangular parallepiped in this illustration, is suspended along a body-diagonal between transmitter and receiver transducers and the input frequency is swept through a given range.

which should be fast, since it must be performed many times. It is the main purpose of the present paper to present such a method, which works for a wide variety of systems, in a simple form which may easily be programmed for a computer.

B. Hamilton's principle

Consider an arbitrarily shaped object with (possibly position dependent) elastic tensor C_{ijkl} and density ρ with a free surface S surrounding a volume V. One forms the kinetic energy density $\mathrm{KE} = 1/2\rho\omega^2 u_i u_i$, the potential energy density $\mathrm{PE} = 1/2 C_{ijkl} u_{i,j} u_{k,l}$, takes their difference, and integrates to get the Lagrangian

$$L = \int_V (\mathrm{KE} - \mathrm{PE}) dV. \tag{1}$$

Here u_i is the ith component of the displacement vector, we use the usual summation convention, and indices following a comma denote differentiation with respect to that coordinate. As usual, we have assumed that the displacements' time dependence is $e^{i\omega t}$.

The following felicitous facts facilitate the computation. If one allows u_i to vary arbitrarily in the volume V and on the surface S, viz., $u_i \to u_i + \delta u_i$, and asks what the variation in L is, the answer is, as the interested reader can easily verify (one integration by parts is needed),

$$L \to L + \delta L, \tag{2}$$

where

$$\delta L = \int_V (\text{elastic wave equation})_i \, \delta u_i \, dV + \int_S (\text{surface traction})_i \, \delta u_i \, dS, \tag{3}$$

plus terms of higher order in δu_i. The elastic wave equation is

$$\rho\omega^2 u_i + C_{ijkl} u_{k,lj} = 0 \tag{4}$$

and the ith component of the surface traction vector is

$$n_j C_{ijkl} u_{k,l}, \tag{5}$$

where $\{n_i\}$ is the unit outer normal to S.

So, apparently due to a mathematical fortuity that may have occurred during a lapse in Murphy's vigilance, the displacement vectors u_i, which are solutions to the elastic wave equation with free boundary conditions on S, are just those points in function space at which L is stationary. This fact suggests the following procedure for obtaining the solutions.

C. Choice of basis

If the computation is to be implemented on a computer, and is to work for a variety of shapes, one should, for reasons soon to become apparent, expand the displacement vector in the simplest possible complete set of functions. There is none simpler than powers of the Cartesian coordinates, so we choose the following set of basis functions:

$$\Phi_\lambda = x^l y^m z^n, \tag{6}$$

where $\lambda = (l,m,n)$ is the function label, a set of three non-negative integers. In terms of this basis we expand the displacements on a truncated set Ω [specified below in (9)]

$$u_i = \sum_{\lambda \in \Omega} a_{i\lambda} \Phi_\lambda, \quad i = 1,2,3. \tag{7}$$

After substituting this into the above expression for the Lagrangian L, the latter can be written ($\mathbf{a}$ becomes a column vector)

$$L = 1/2\omega^2 \mathbf{a}^T E \mathbf{a} - 1/2 \mathbf{a}^T \Gamma \mathbf{a}, \tag{8}$$

where E and Γ are matrices whose order R is determined by Ω, which is specified by the condition

$$l + m + n \leqslant N, \tag{9}$$

viz. $R = 3(N+1)(N+2)(N+3)/6$. [The initial factor of 3 here corresponds to the three coordinates x, y, and z. The other factors are the number of ways (9) can be realized for non-negative l, m, and n.] To keep the size of the matrices within manageable limits we must clearly be restrained in our choice of N.

The matrix E has elements

$$E_{\lambda i \lambda' i'} = \delta_{ii'} \int_V \Phi_\lambda \rho \Phi_{\lambda'} \, dV. \tag{10}$$

If we had chosen $\{\Phi_\lambda\}$ to be a set orthonormal with respect to the weight function ρ, then E would have been the unit matrix, which would have simplified some subsequent manipulations. But then we would have had to choose a different $\{\Phi_\lambda\}$ for each shape, and for each different density ρ, which can be a function with arbitrary position dependence, and we would not be able to express the required matrix elements which follow in closed form. The moderate penalty exacted by a nondiagonal E is more than compensated by the other advantages concomitant with (6).

The matrix Γ has elements

$$\Gamma_{\lambda i \lambda' i'} = C_{iji'j'} \int_V \Phi_{\lambda,j} \Phi_{\lambda',j'} \, dV. \tag{11}$$

Again, the volume integrals that appear here are quite tractable for many shapes V if the choice (6) is made, which is not the case for other basis sets.

D. Generalized eigenvalue equation

The expression (8) for the Lagrangian (1) is stationary, according to (3), for the displacements u_i that are solutions of the free-vibration problem. So the solutions may be obtained by setting the derivatives of (8) with respect to each of the R amplitudes $a_{i\lambda}$ equal to zero. This yields the following matrix eigenvalue equation:

$$\omega^2 E \mathbf{a} = \Gamma \mathbf{a}. \tag{12}$$

The matrix E, although not diagonal, as it would be if we had chosen an orthonormal basis, is symmetric and positive definite, and Γ is symmetric, so that a standard eigenvalue–eigenvector subroutine package (RSG in EISPACK[13,14]) can be used to solve (12) as easily and nearly as quickly as it could if E had been diagonal.

II. EXAMPLES

A. The potato

For our choice of $\{\Phi_\lambda\}$ the matrix elements of E and of Γ are all of the form

$$f(p,q,r) = \int_V x^p y^q z^r \, dV, \tag{13}$$

where p, q, and r are non-negative integers. This integral can be evaluated analytically for a variety of V's, including one which we call the potato, for want of a better name. The potato is constructed by choosing six different semiaxes $(d_{1+}, d_{1-}, d_{2+}, d_{2-}, d_{3+}, d_{3-})$, and filling each octant of the Cartesian coordinate system (x,y,z) with a (different) ellipsoidal segment. Figure 2 shows a contour plot of the upper half of a typical potato with semiaxes given below.

The integral (13) for this shape is just the sum over the octants of terms of the form

$$f_8(p,q,r) = \{1,\pi/2\} d_{1+}{}^{p+1} d_{2+}{}^{q+1} d_{3+}{}^{r+1} \times (p-1)!!(q-1)!!(r-1)!!/(p+q+r+3)!!, \tag{14}$$

which is the integral (13) on the $(+++)$ octant. (It is an integral representation for the beta function.[15]) The curly bracket is unity if two or three of the integers p, q, and r are odd; otherwise it is equal to $\pi/2$. The double factorial is, as usual, the product of alternate positive integers up to the argument, with $(0)!! = (-1)!! = 1$. The integrals on the other octants have the same form, but have a sign that depends in an obvious way on whether p, q, and r are even or odd.

1. Comparison with measured potato frequencies

Table I lists some of the computed frequencies ($f = \omega/2\pi$) of the normal modes of an aluminum half-potato with measured density $\rho = 2.7065$ g/cm^3 and Lamé parameters $\lambda = 0.54\times10^{12}$, $\mu = 0.27\times10^{12}$ erg/cm^3 (Poisson's ratio $= 1/3$) appropriate to Al ($C_{11} = \lambda + 2\mu$, $C_{12} = \lambda$, $C_{44} = \mu$, using the Voight contracted notation for the elastic constants), and semiaxes $(d_{1+},\ldots,d_{3-})$ $= (2,5,4,1,3,0)$ in. We have adjusted λ, but not Poisson's ratio, so that the average of the lowest ten frequencies is equal to that measured. Omitted are the zero frequencies, of which there are always six, corresponding to three translations and three rotations. These frequencies were computed by solving the generalized eigenvalue problem (12) with $N = 6$, 7, 8, and 9.

TABLE I. Measured and calculated Al potato frequencies (Hz).

Mode	Measured	$N=6$	$N=7$	$N=8$	$N=9$
1	9914	9925	9923	9922	9922
2	10391	10413	10410	10409	10408
3	13513	13484	13481	13480	13480
4	15802	15860	15841	15837	15836
5	17064	17116	17091	17085	17083
6	17285	17270	17268	17268	17268
7	17892	17903	17885	17881	17880
8	19225	19244	19195	19184	19181
9	20999	21060	21045	21038	21037
10	21800	21936	21842	21815	21808
20	28933	29258	29038	28985	28968
30	34866	36230	35423	35077	34958
Cray-1 CPU time		3s	7s	15s	29s
		$R=252$	$R=360$	$R=495$	$R=660$

Comparison of the computed frequencies in the corresponding columns shows that $N = 6$ gives 1/2% or better accuracy for the lowest ten lines, and larger N's give much better accuracy. (Notice that the rows are monotonically decreasing sequences, as is required by Cauchy's inequality.[16]) Convergence is slower for this shape, which has sharp edges, than for smooth-surfaced objects. It should be emphasized that, although this potato is elastically isotropic, it is no more difficult and takes little more computer time to calculate the frequencies (and eigenfunctions) for the general elastic potato with 21, or even 81 independent C_{ij}'s.

Figure 3 is a photograph of this aluminum potato, which was fabricated using a numerically controlled ball mill. The reason that $d_{3-} = 0$ is that the half-potato has a plane surface for measurement references, which makes it easier to machine. The surface quality is 32 μin. rms, which is also a limit on the accuracy with which it reproduces the nominal composite-ellipsoidal shape.

Transducers were cemented to the flat side of this object, and its resonant frequencies were measured.[17] They are listed in the second column of Table I. The measurement errors, as gauged by the scatter in resonant frequencies when the suspension and transducer positions are changed, are comparable to the rms difference between measured and calculated frequencies, which is 0.16% for the lowest ten resonances. The above choice of λ minimizes the error, and probably amounts to as good a determination of the elastic constants of this Al alloy as is available.

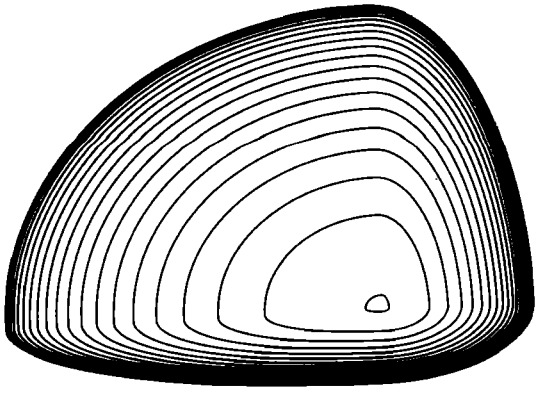

FIG. 2. Elevation contours of the half-potato described in the text. The bottom of this object is flat. It comprises four ellipsoidal segments.

B. The tetrahedron, the octahedron, and the prism

Another object of low symmetry is a tetrahedron whose faces comprise the yz, xz, xy planes and the plane

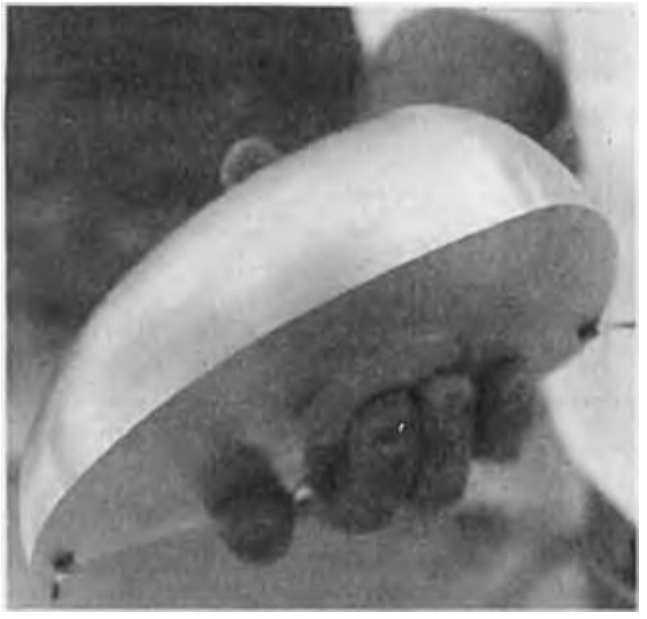

FIG. 3. Photograph of the machined aluminum half-potato that was made by a numerically controlled ball mill and whose ultrasonic resonant frequencies were measured. This object weighs 2438.4 g, and its density is 2.7065 g/cm^3. Two 1/4 in.-diam transducers cemented to the flat side are visible here.

$x/a + y/b + z/c = 1$. This is the so-called corner prism, and one can easily[18] work out (13) for this shape. It is

$$f(p,q,r) = a^{p+1}b^{q+1}c^{r+1}p!q!r!/(p+q+r+3)!. \quad (15)$$

This prism occupies the $(+++)$ octant and, just as the potato was formed from eight ellipsoidal segments, one can make an octahedron by piecing together eight of these prisms.

The cylindrical prism bounded by the planes $x=0$, $y=0$, $z=0$, $z=c$, and $x/a + y/b = 1$ has

$$f(p,q,r) = a^{p+1}b^{q+1}c^{r+1}p!q!/(p+q+2)!(r+1), \quad (16)$$

and it is possible, albeit sometimes tedious and not always easy, to work out many other polyhedric shapes.

III. SYMMETRIES

The potato is an object of low symmetry. If we go to the other extreme, the ellipsoid (which is the potato for $d_{i+} = d_{i-}$, $i = 1,2,3$), we can speed up the calculation immensely by exploiting the threefold inversion symmetry $x \to -x$, $y \to -y$, $z \to -z$, which then obtains. Now we require that the symmetry of the crystal be orthorhombic or better (i.e., that off-diagonal elements $C_{ij} = 0$ if either i or j is 4, 5, or 6). Then, by inspection of the PE in (1) (see Ohno[4]) we see that, if u_x is characterized by a parity triplet $(-\lambda,\mu,\nu)$ [where $\lambda = (-1)^l, \mu = (-1)^m, \nu = (-1)^n$], then the Γ matrix only connects this u_x with u_y and u_z having the following parities:

$$u_x:(-\lambda,\mu,\nu), \quad u_y:(\lambda,-\mu,\nu), \quad u_z:(\lambda,\mu,-\nu). \quad (17)$$

Therefore, the Γ matrix degenerates into a block-diagonal matrix with eight blocks, each characterized by one parity triplet, say the parity of u_x. We label this parity as follows:

$$\begin{array}{cccccccccc} k= & 1 & & 2 & & 3 & & 4 & & 5 \\ (-\lambda,\mu,\nu)= & (+,+,+) & & (+,+,-) & & (+,-,+) & & (+,-,-) & & (-,+,+) \end{array} \quad \begin{array}{cccc} 6 & & 7 & & 8, \\ (-,+,-) & & (-,-,+) & & (-,-,-). \end{array} \quad (18)$$

Because of the high symmetry the modes for each k value (18) are uncoupled (i.e., k is a "good quantum number"), and with $N = 7$, as in the potato, the largest order for which we have to solve the eigenvalue problem (12) is $R = 60$, in contrast to $R = 360$ to get the same accuracy in the potato, although it must be added that now we need to solve an eigenvalue problem for each of the eight k values.

The layered sphere (or ellipsoid), which might be used as a model for oscillations of the earth, may also be studied using linear combinations of (14) (one term for each layer in the model) to represent $f_s(p,q,r)$. We have computed frequencies by this method for a model consisting of a core plus a crust (both elastically isotropic) and have found, by comparing the results with an exact calculation using spherical Bessel functions and spherical harmonics (eigenfunctions of the elastic wave equation in spherical coordinates), that the accuracy of the present method is excellent even for small N if the mismatch of the acoustic impedances at the boundary is not too large.

IV. OTHER EXAMPLES WITH THREEFOLD INVERSION SYMMETRY

A. The rectangular parallelepiped

The $2d_1 \times 2d_2 \times 2d_3$ rectangular parallelepiped is the shape considered by Demarest[3] and by Ohno[4] (both of whom used Legendre polynomials for their basis set $\{\Phi_i\}$) The numerical procedure to be followed here is identical to that for the ellipsoid. Only (14) is changed; it is now

$$f(p,q,r) = 8d_1^{p+1}d_2^{q+1}d_3^{r+1}/(p+1)(q+1)(r+1). \quad (19)$$

B. The cylinder

The right circular (or elliptical) cylinder also has threefold inversion symmetry. Again the numerical procedure is the same as before with

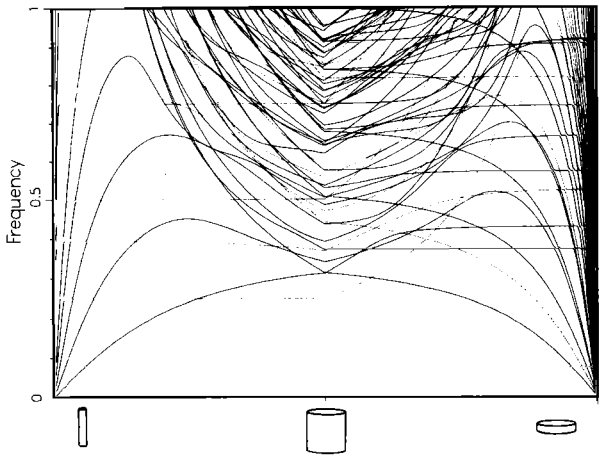

FIG. 4. Low-lying resonant frequencies of a family of cylinders. On the left half of the plot, the height of the cylinder is held constant at 2, and the aspect ratio (diameter/height) is varied linearly from 0 at the origin to 1 at the center of the plot. Then the diameter is held constant at 2 on the right half, and the height is decreased to 0 at the right end of the abscissa. There are a number of noteworthy features on this plot. First, on the left, there are modes whose frequencies are independent of the cylinder's diameter for any aspect ratio. These have frequencies that are integral multiples of $(\mu/\rho)^{1/2}/2h = 1/4$, where h is the height of the cylinder. They are the torsional modes[19] with h equal to multiples of half-wavelengths. Second, also on the left, there are two modes whose frequencies are independent of diameter as the diameter becomes small. These are the compressional "Young's modulus" modes with frequencies integral multiples of $(E/\rho)^{1/2}/2h = 0.395$, where $E =$ Young's modulus $= \mu(3\lambda + 2\mu)/(\lambda + \mu) = 5/2$. Third, on the right, one finds two modes with frequencies independent of h even for large h. Their frequencies are close (but not within our computational uncertainty) to being given by $J_0(2\pi f) = 0$. Finally, on the right again, there are many modes whose frequencies become independent of h as h becomes small. They must be describable as vibrations of an elastic membrane with free edges, and might therefore be analytically tractable.

$$f(p,q,r) = 4\pi\, d_1{}^{p+1}\, d_2{}^{q+1}\, d_3{}^{r+1} \times (p-1)!!(q-1)!!/(r+1)(p+q+2)!!, \tag{20}$$

where $2d_3$ is the height and d_1, d_2 are the semiaxes of the elliptical cross section of the cylinder. We have computed the resonant frequencies for cylinders with various aspect ratios. The results are exhibited in Fig. 4, in which we have taken $N = 8$, unit density, and isotropic elasticity with unit Lamé parameters.

C. The spheroid

Very similar to the cylinder spectrum is that of the spheroid. Here, $f(p,q,r)$ is given by (14) for this shape, and its spectrum as a function of aspect ratio is shown in Fig. 5, with the prolate limit on the left, the sphere in the center, and the oblate limit on the right. Differences that stand out between this plot and Fig. 4 for the cylinder are: (1) the massive degeneracy of resonances in the spherical case and (2) the fact that many of the cylinder modes are rigorously independent of aspect ratio, not the case for the spheroid.

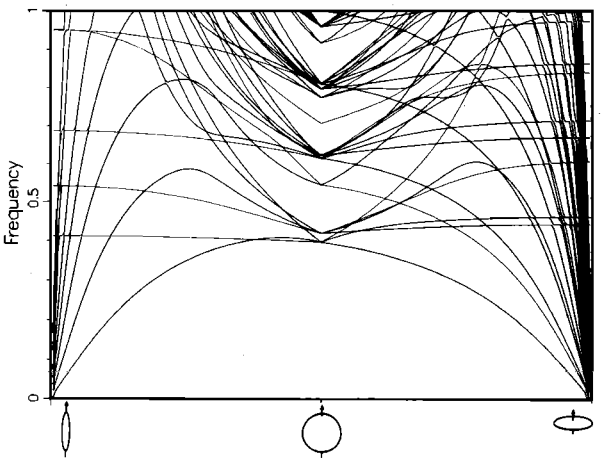

FIG. 5. Like Fig. 4, but for a family of spheroids. The sphere of unit radius is at the center, prolate spheroids with radius proportional to the abscissa on the left, culminating with the needle of length 2. To the right of center are oblate spheroids with unit radius ending with the zero-thickness pancake. In contrast to the cylinder, there are no frequencies here that are trivially calculable.

V. LESS SYMMETRIC OBJECTS

Intermediate between the potato and the ellipsoid, as far as symmetry is concerned, are the following objects that break the $z \to -z$ symmetry while retaining the x and y symmetries. Now the Γ matrix does not break up into eight diagonal blocks, as it did in for the ellipsoid, but only into four, since z parity is no longer conserved. From (16), we see that $k = 1$ mixes with $k = 2$, $k = 3$ mixes with $k = 4$, $k = 5$ with 6, and 7 with 8, so that the diagonal blocks can be labeled $k = 1$, 3, 5, and 7.

A. The sandwich

By the sandwich, we mean a rectangular parallelepiped in which there is a material discontinuity in the z direction, as illustrated in Fig. 6. For $z < b$ the elastic constants and the density are C_{ij}^{-}, ρ^{-}, and for $z > b$ they are C_{ij}^{+}, ρ^{+}. The changes in $f(p,q,r)$ are trivial and obvious. Some frequencies for this system are illustrated in Fig. 7, in which the abscissa

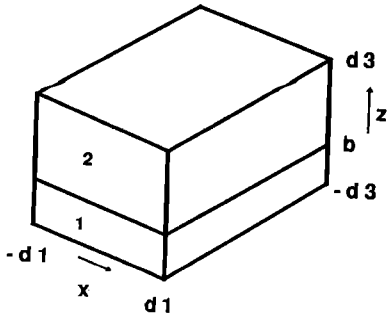

FIG. 6. A rectangular parallelepipedal open-faced sandwich. Material 1 occupies the part of V with $z < b$, material 2 occupies the part with $z > b$. The origin is at the center of the block.

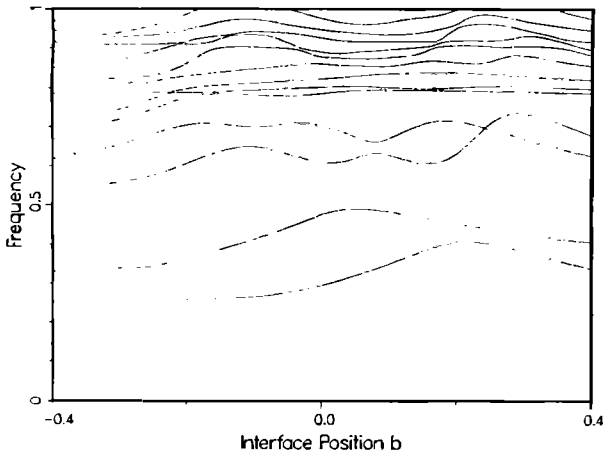

FIG. 7. The $k = 7$ normal-mode frequencies of the object illustrated in Fig. 6. The densities and Lamé parameters of the two materials are related as discussed in the text, so that the frequencies are identical at the right and left extremes, where the object is all stiff and heavy versus all soft and light. It is interesting that the third and fourth resonances cross once, and avoid crossing twice, so that the symmetries of these modes apparently change as b does. Here $(d_1,d_2,d_3) = (0.2,0.3,0.4)$, $(\rho,\lambda,\mu) = (2,0.4,0.4)$, $(10,2,2)$ in the bottom and top parts, respectively.

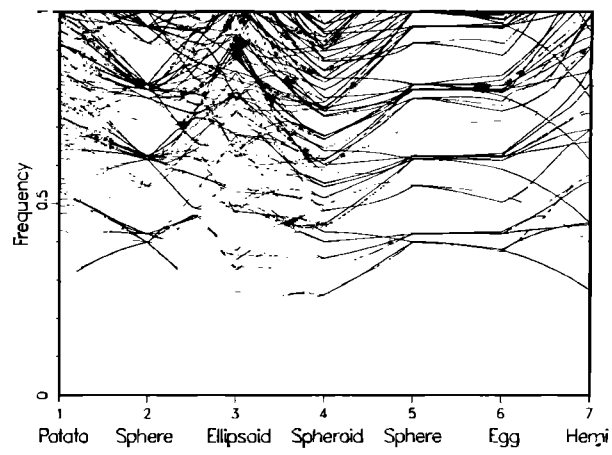

FIG. 8. Frequency spectra of a number of objects in the potato family. The seven stations correspond to shapes as labeled, with semiaxes as given in Table II. The sphere frequencies agree well with those in the literature for these material parameters (Poisson's ratio = 1/4).[20] The dimensional parameters $d_{1+},d_{1-},\ldots,d_{3-}$ are interpolated linearly between the seven stations here. Several interesting features invite comment. First, the potato has no degenerate lines, because of its low symmetry, and the sphere, conversely, has few lines that are nondegenerate. The ellipsoid has no degeneracies, and the spheroid, the egg, and the hemisphere (all being rotationally symmetric) do, but never more than doubly degenerate lines. Small deviations from the sphere in the egg direction do not change any of the frequencies to first order, because d_{3+} increases as much as d_{3-} decreases, compensating one another as far as affecting resonant frequencies is concerned. As in several other figures, apparent avoided crossings on this plot should be viewed with suspicion because the plotting program does not interchange line identities when physically the modes do, in fact, cross. Spectra are computed for 241 abscissa values here and elsewhere, which sets the scale on which avoided crossings may be spurious.

is b, the z position of the interface. We have chosen the densities and elastic constants to scale together; i.e., $\rho^+ = \alpha\rho^-$ and $C_{ij}^+ = \alpha C_{ij}^-$ with $\alpha = 5$, so that the frequencies, when the block is all one material, are identical to those when it is all the other material, although they vary considerably for intermediate compositions, and the identities of some of the modes are exchanged in the process.

B. The egg, the hemisphere, and the bell

The egg is a special case of the potato with $d_{1+} = d_{1-}$, $d_{2+} = d_{2-}$. It has twofold inversion symmetry; whereas the degeneracies of the spherical case are broken completely by the potato (as well as by the ellipsoid), they are only partly broken by the egg and the spheroid.

The hemisphere is a special case of the egg with $d_{3-} = 0$. The bell is a hemispheroid with a concentric hemispheroidal hole in it, formed by superimposing on the original hemispheroid a smaller one with negative density and elastic constants.

In Fig. 8 are shown resonant frequencies for a family of shapes: the potato, the ellipsoid, the spheroid, the sphere, the egg, and the hemisphere. The stations along the abscissa are labeled: The semiaxes characterizing the various shapes are listed in Table II. These parameters are linearly interpolated between the stations. Isotropic material with unit density and Lamé parameters is again assumed.

To illustrate the possibility of tuning the timbre of a bell by adjusting the bell's proportions, we show, in Fig. 9, the spectra of a family of bells. The abscissa is the logarithm of the aspect ratio $2d_1/d_{3+}$, which varies from 1/10 at the extreme left to unity in the middle (half a 2:1 prolate spheroidal shell) to 10 at the right-hand side. Thus, on the left, we have a chimelike object, and on the right we have something close to a cymbal. The semiaxes of the inner surface are 0.9 of those for the outside surface.

C. The cone and the pyramid

The cone fits easily into our recipe if we take its point to be at $z = 0$, and its base to be at $z = d_3$. Then, the cross sections of the cone parallel to the xy plane will be ellipses whose semiaxes are proportional to z. For this object, we find

$$f(p,q,r) = 2\pi d_1^{\,p+1} d_2^{\,q+1} d_3^{\,r+1} \times (p-1)!!(q-1)!!/(p+q+2)!!(p+q+r+3). \quad (21)$$

TABLE II. Semiaxes for the objects in Fig. 8.

Object	d_{1+}	d_{1-}	d_{2+}	d_{2-}	d_{3+}	d_{3-}
1. Potato	0.25	1.0	0.5	1.25	0.75	1.5
2. Sphere	1.0	1.0	1.0	1.0	1.0	1.0
3. Ellipsoid	0.5	0.5	1.0	1.0	1.5	1.5
4. Spheroid	1.0	1.0	1.0	1.0	1.5	1.5
5. Sphere	1.0	1.0	1.0	1.0	1.0	1.0
6. Egg	1.0	1.0	1.0	1.0	1.5	0.5
7. Hemisphere	1.0	1.0	1.0	1.0	1.0	0.0

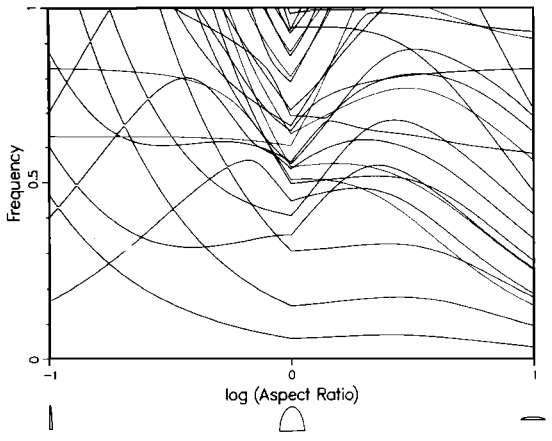

FIG. 9. Spectra of an idealized family of bells. These are hemispheroidal shells, with inner semiaxes always 0.9 of the outer ones. The material is our standard isotropic elastic medium with $\lambda = \mu = \rho = 1$. The abscissa is $\log_{10}$ (bell diameter/bell height). The height is kept constant at unity on the left half of the plot, and the diameter is kept constant on the right half. It should be noted that one cannot tell what a bell will sound like by examining a plot like this, because, for one thing, the extent to which a given mode will be excited depends on its amplitude at the clapper strike point. This information is available to us, but is more labyrinthine than the frequencies. Many other factors also enter, such as the Q's of the modes and their coupling to the air.

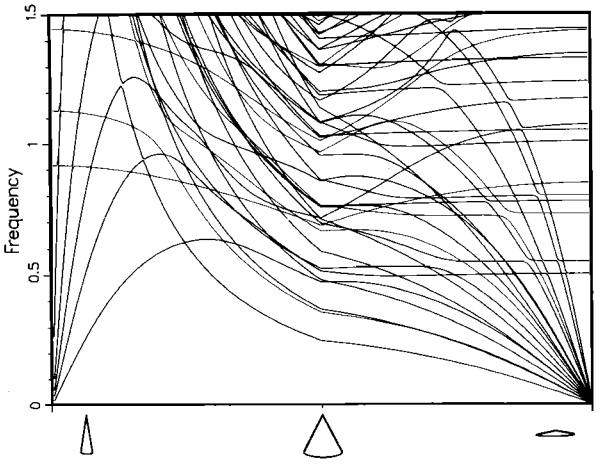

FIG. 10. These are the spectra for a family of right-circular cones. The height h is 2 at the left extreme, and the diameter is 0. The diameter increases linearly along the abscissa while h remains constant until at the center the aspect ratio is 1. Then the diameter is held constant at 2 while h decreases to 0 at the right extreme. There are some intriguing features on this graph, namely that at both the needle limit and the discus limit some of the frequencies are independent of the vanishing dimension, leading one to expect that a simple analytic description should be possible.

Likewise, the pyramid has its point at $z = 0$ and its $2d_1 \times 2d_2$ base at $z = d_3$. For it,

$$f(p,q,r) = 4{d_1}^{p+1}{d_2}^{q+1}{d_3}^{r+1}/(p+q+r+3)(p+1)(q+1). \quad (22)$$

Figure 10 displays the resonant frequencies for a cone made of our standard isotropic material with $\lambda = \mu = \rho = 1$.

D. The cylinder with a skewed end

A cylinder bounded by the ellipse $(x/d_1)^2 + (y/d_2)^2 = 1$ and the planes $z = 0$ and $z = d_3(1 + \alpha x/d_3)$ has

$$f(p,q,r) = 2\pi(q-1)!!{d_1}^{p+1}{d_2}^{q+1}{d_3}^{r+1}g(p,q,r), \quad (23)$$

where

$$g(p,q,r) = \sum_{m=0}^{r+1} (\alpha d_1/d_3)^m r!(p+m-1)!! \times [m!(r+1-m)!(p+q+m+2)!!]^{-1} \quad (24)$$

and

$$\alpha = \tan\theta$$

is the slope of the top of the cylinder, which makes an angle θ with the horizontal. Note that this object breaks both the $x \to -x$ and $z \to -z$ symmetries, so the Γ matrix comprises only two diagonal blocks.

VI. ANISOTROPY

Since the word "anisotropic" appears in the title of this paper, it is fitting that we give some results for systems with anisotropic elastic constants. The simplest anisotropic material has transverse isotropy, or hexagonal symmetry. There are now five independent elastic constants. If the sixfold axis is in the z direction they are $C_{33}, C_{12}, C_{13} = C_{23}, C_{44} = C_{55}$, and C_{66}, with $C_{11} = C_{22} = C_{12} + 2C_{66}$. To illustrate the effects of anisotropy, we will use a set of elastic constants, parametrized with a number g, close to our standard isotropic set, namely,

$$C_{11} = C_{22} = 3, \quad C_{33} = 3g, \quad C_{12} = C_{66} = 1, \quad C_{13} = C_{23} = C_{44} = C_{55} = g, \quad (25)$$

when the symmetry axis is in the z direction.

A. The anisotropic cone

To illustrate the effects on the spectrum of variation of the magnitude of the anisotropy, we consider a right circular cone with unit aspect ratio. In Fig. 11 are shown the normal-mode frequencies of this object as functions of anisotropy. Here, $g = 1$ at the center, where the material is isotropic, and g increases in both directions away from the center. On the left half of the plot the sixfold axis is the z axis, so rotational symmetry about the z axis obtains, and is evidenced by many twofold degeneracies. On the right half the sixfold axis is the x axis (so the elastic constants are obtained from those above by interchanging 1 with 3 and 4 with 6).

B. The anisotropic spheroid

To illustrate the effects of varying the direction of anisotropy with a fixed magnitude, we consider an oblate spheroid with aspect ratio 2. In Fig. 12 is shown the vibrational spectrum of this object as a function of angle between the spheroid axis and the sixfold axis, when $g = 3.5$. To compute these curves one rotates the elastic tensor C_{ijkl} about the y axis through angles given by the value of the abscissa. In the

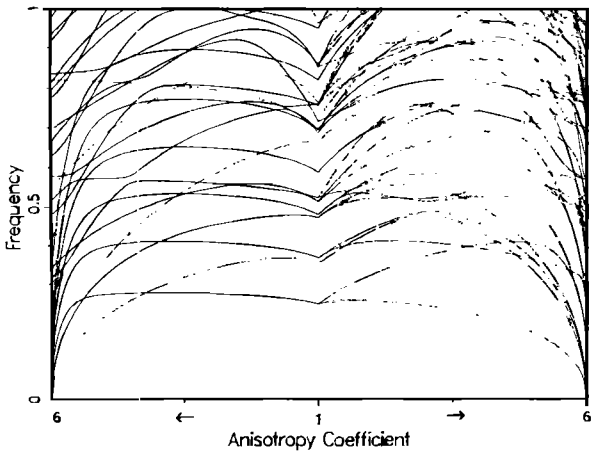

FIG. 11. These are the spectra for a right-circular cone with unit aspect ratio as functions of the anisotropy parameter g discussed in the text. At the center ($g = 1$) the material is elastically isotropic. As one goes to the left it has hexagonal symmetry with the sixfold axis in the z direction, so that rotational symmetry about the z axis holds, and the anisotropy parameter increases linearly to 6 at the left extreme. As one goes to the right from the center the sixfold axis is in the x direction, so the system lacks rotational symmetry. The degeneracies characteristic of rotational symmetry disappear when one crosses the center from left to right. Another interesting point is that some frequencies become imaginary at $g = 6$. The condition that the energy of the system be positive definite is that $\det|C_{ij}| > 0$. One can easily compute $\det|C_{ij}| = 4g^3(6 - g)$, so one would expect catastrophe not only for $g > 6$, but also, not unexpectedly, for $g < 0$.

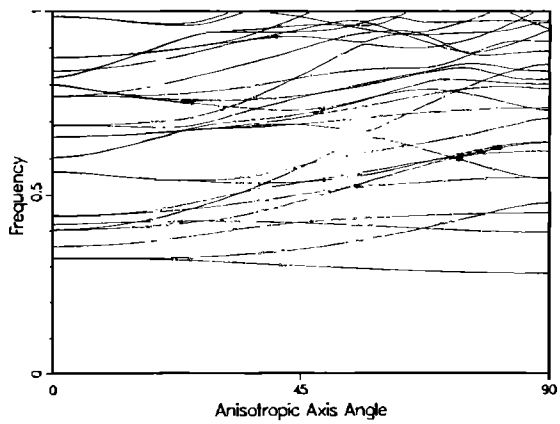

FIG. 12. These are the spectra for a 2:1 oblate spheroid composed of the same material as that in the preceding figure, i.e., an anisotropic hexagonal elastic tensor, with $g = 3.5$. The abscissa is the angle between the axis of the spheroid and the sixfold axis: They are parallel on the left, perpendicular on the right. Most of the states are twofold degenerate when the axes are parallel: Otherwise there are no degeneracies.

process, of course, one loses the advantages of threefold symmetry of the spheroid, and the computation takes as long as that for the anisotropic cone.

VII. DISCUSSION

Our computational scheme, which we call the *xyz* algorithm on account of Eq. (6), its basic distinction from the Demarest[2] algorithm, enables the calculation of normal modes for many classes of systems that have not been computed before by any method (even those as simple as the isotropic spheroid or cone, let alone the anisotropic potato), and could be calculated only with great difficulty by existing methods. The *xyz* algorithm, by its nature, is no more difficult to apply to general anisotropic systems with 21 (or even 81, the total number of elements of C_{ijkl}) independent elastic constants than to isotropic ones, and allows one easily to compute a wider variety of shapes than any other.

Although we have displayed only the resonant frequencies that these calculations have yielded, the same EISPACK subroutines also give the eigenvectors $a_{i\lambda}$ in (7). Thus the elastic displacements are known, and with enough persistence and determination, we could have shown vibrational shapes for each of the modes. But there are too many of them, so we will show none.

We believe we have demonstrated that the *xyz* algorithm is capable of quickly and accurately yielding the low-lying resonant frequencies for a wide variety of shapes with inhomogeneities and few restrictions on anisotropy. But perhaps its greatest virtue is its extreme simplicity when compared to other schemes that are less versatile, accurate, or speedy.

ACKNOWLEDGMENT

This work was supported by the USDOE.

APPENDIX

Here we give the listing of a Fortran program that will compute the normal-mode frequencies (and, with trivial modifications, the eigenfunctions, too) for all the objects we have discussed in this paper. This code does not exploit any of the symmetries of shape or elasticity tensor, and is therefore much slower than one that does for objects with symmetries, as is discussed in Sec. III.

```
        The program is named for the basis functions it uses.
      PROGRAM XYZ
        The arrays are dimensioned 252 here, sufficient for N=6.
      DIMENSION GAMMA(252,252),E(252,252),W(252),FV(252),FW(252),
     & C(3,3,3,3), LB(252),MB(252),NB(252),IC(252)
        The data following is the elastic tensor C_ijkl for our standard
        isotropic material.  Any homogeneous anisotropy can be
        described by simply changing these data to include up to 81
        different elastic constants, for a general substance in the
        presence of magnetic fields.
      DATA C/3.,3*0.,1.,3*0.,1.,0.,1.,0.,1.,7*0.,1.,3*0.,1.,3*0.,1.,0.,1.,5*0.,1.,
     & 3*0.,3.,3*0.,1.,5*0.,1.,0.,1.,3*0.,1.,3*0.,1.,7*0.,1.,0.,1.,0.,1.,3*0.,1.,3*0.,3 /
      DATA RHO/1./
      TWOPI=2.*ACOS(-1.)
      PRINT*,'PLEASE INPUT NN'
      READ*,NN
        The next 13 lines assign an index IG to each basis function (6).
      IG=0
      DO 1 I=1,3
      DO 2 L=1,NN+1
      DO 2 M=1,NN+1
      DO 2 N=1,NN+1
      IF(L+M+N.GT.NN+3) GO TO 2
      IG=IG+1
      IC(IG)=I
      LB(IG)=L-1
      MB(IG)=M-1
      NB(IG)=N-1
    2 CONTINUE
    1 CONTINUE
      NR=IG
```

```
*In the next 11 statements the elements of the E and Γ
*matrices are computed.
      DO 3 IG=1,NR
      DO 3 JG=IG,NR
      I=IC(IG)
      J=IG(JG)
      LS=LB(IG)+LB(JG)
      MS=MB(IG)+MB(JG)
      NS=NB(IG)+NB(JG)
      GAMMA(IG,JG)=
     & C(I,1,J,1)*FLOAT(LB(IG)*LB(JG))*F(LS-2,MS,NS)
     & +C(I,2,J,2)*FLOAT(MB(IG)*MB(JG))*F(LS,MS-2,NS)
     & +C(I,3,J,3)*FLOAT(NB(IG)*NB(JG))*F(LS,MS,NS-2)
     & +(C(I,1,J,2)*FLOAT(LB(IG)*MB(JG))+C(I,2,J,1)*
     & FLOAT(MB(IG)*LB(JG)))*F(LS-1,MS-1,NS)
     & +(C(I,1,J,3)*FLOAT(LB(IG)*NB(JG))+C(I,3,J,1)*
     & FLOAT(NB(IG)*LB(JG)))*F(LS-1,MS,NS-1)
     & +(C(I,2,J,3)*FLOAT(MB(IG)*NB(JG))+C(I,3,J,2)*
     & FLOAT(NB(IG)*MB(JG)))*F(LS,MS-1,NS-1)
      GAMMA(JG,IG)=GAMMA(IG,JG)
      IF(I.EQ.J) E(IG,JG)=F(LS,MS,NS)
3     E(JG,IG)=E(IG,JG)
*The next line solves the eigenvalue problem (12) using the
*EISPACK[13,14] subroutine RSG.
      CALL RSG(252,NR,GAMMA,E,W,0,Z,FV,FW,IERR)
*Now obtain the frequencies from the eigenvalues. If C_ijkl is in
*10^12 dynes/cm^2, ρ is in g/cm^3, and dimensions are in cm, then
*frequencies W are in MHz.
      DO 4 I=1,NR
4     W(I)=SQRT(AMAX1(0.,W(I))/RHO)/TWOPI
*The lowest 36 frequencies are printed out: the first 6 of
*these are always zero if Γ is positive.
      PRINT*,"FREQUENCIES FOR CORNER PRISM, NN= ",NN
      PRINT 101,(W(I),I=1,36)
101   FORMAT(6G12.5)
      END
*Next is a function subprogram for f(p,q,r) for the corner prism
*(Eq. 15). It is straightforward here to substitute function
*subprograms for any of the other objects we have
*considered.
      FUNCTION F(IP,IQ,IR)
      DATA A,B,C/3*1./
      F=A**(IP+1)*B**(IQ+1)*C**(IR+1)*
     & FACT(IP)*FACT(IQ)*FACT(IR)/FACT(IP+IQ+IR+3)
      RETURN
      END
*Factorial subprogram follows.
      FUNCTION FACT(N)
      FACT=1.
      IF(N.LT.2) RETURN
      DO 1 I=2,N
      FACT=FACT*FLOAT(I)
      RETURN
      END
```


[1] R. Holland, J. Acoust. Soc. Am. **43**, 988 (1968).
[2] H. H. Demarest, Jr., Bachelor's thesis, Reed College, Portland, OR (1969).
[3] H. H. Demarest, Jr., J. Acoust. Soc. Am. **49**, 768 (1971).
[4] I. Ohno, J. Phys. Earth **24**, 355 (1976).
[5] Y. Sumino, I. Ohno, T. Goto, and M. Kumazawa, J. Phys. Earth **24**, 263 (1976).
[6] I. Ohno, S. Yamamoto, O. L. Anderson, and J. Noda, J. Phys. Chem. Solids **47**, 1103 (1986).
[7] A. Migliori, W. M. Visscher, S. E. Brown, Z. Fisk, S.-W. Cheong, B. Alten, E. T. Ahrens, K. A. Kubat-Martin, J. D. Maynard, Y. Huang, D. R. Kirk, K. A. Gillis, H. K. Kim, and M. H. W. Chan. Phys. Rev. B **41**, 2098 (1990).
[8] A. Migliori, W. M. Visscher, S. Wong, S. E. Brown, I. Tanaka, H. Kojima, and P. B. Allen. Phys. Rev. Lett. **64**, 2408 (1990).
[9] E. Mochizuki, J. Appl. Phys. **63**, 5668 (1988).
[10] S. Isoda, H. Oda, I. Suzuki, and K. Seya, Tohoku Geophys. J. **32**, 55 (1990).
[11] See the famous paper, "Can One Hear the Shape of a Drum?" by M. Kac, Am. Math. Month. **73**, 1 (1966). For more recent work, see M. H. Protter, SIAM Rev. **29**, 185 (1987).
[12] A. Stekel, J. L. Sarrao, T. M. Bell, Ming Lei, R. G. Leisure, W. M. Visscher, and A. Migliori (to be published).
[13] B. T. Smith, J. M. Boyle, J. J. Dongarra, B. S. Garbow, Y. Ikebe, V. C. Klema, and C. B. Moler, "Matrix Eigensystem Routines—EISPACK Guide," in *Lecture Notes in Computer Science No. 6*, edited by G. Goos and J. Hartmanis (Springer, New York, 1976).
[14] B. S. Garbow, J. M. Boyle, J. J. Dongarra, and C. B. Moler, "Matrix Eigensystem Routines—EISPACK Guide Extension," in *Lecture Notes in Computer Science No. 51*, edited by G. Goos and J. Hartmanis (Springer, New York, 1977).
[15] *Handbook of Mathematical Functions*, edited by M. Abramowitz and I. A. Stegun (National Bureau of Standards Applied Mathematics Series No. 55, Washington, DC, 1965), p. 258.
[16] M. Marcus, *Basic Theorems in Matrix Theory* (National Bureau of Standards Applied Mathematics Series No. 57, Washington, DC, 1960), p. 12.
[17] F. Birch, J. Geophys. Res. **80**, 756 (1974). This paper, concerned with vibrations of steel, glass, and rock spheres, provides a precedent for comparing measured and computed normal-mode frequencies of objects with simple geometries.
[18] This is an exercise that we leave for the interested reader. Hint: Start by evaluating the form factor $\langle \exp(k.r) \rangle$ for the tetrahedron.
[19] L. D. Landau, E. M. Lifshitz, A. M. Kosevich, and L. P. Pitaevskii, *Theory of Elasticity* (Pergamon, New York, 1986).
[20] H. Lamb, Proc. Math Soc. **13**, 189 (1882).